JCSE The Journal of Corrosion Science and Engineering

Century 21st Corrosion Science

Volume 6 paper C021

Mechanisms of Zirconium Alloy Corrosion in Nuclear Reactors

B. Cox
Centre for Nuclear Engineering,
University of Toronto,
Toronto, ON, Canada, M5S 3E4

Abstract

The extent to which irradiation in a nuclear reactor core accelerates the corrosion of zirconium alloys has always been a concern. It was expected that radiation induced defects in the protective zirconia film would enhance diffusion controlled oxide growth, and lead to early breakdown of the protective oxide. Studies of irradiated oxide films (>10yr. in reactor) have found no evidence for irradiation induced defects in the critical region of the oxide close to the metal/oxide interface. This suggests that recombination of the point defects produced must be essentially complete. Enhanced oxide growth in-reactor must, therefore, involve other processes. Early studies showed that electronic conduction in the oxide, rather than oxygen diffusion was the rate determining process. In-reactor, therefore, the enhanced conductivity of the oxide film should relax this limitation on the oxide growth rate. Under such conditions galvanic currents between the zirconium alloy and a dissimilar metal could then become significant as well. That these two effects can operate simoultaneously and independently was shown in experiments in the ATR at low temperatures. Specimens were contained in aluminum holders, and experienced both cathodic hydriding in areas of proximity to Al (galvanic), and enhanced anodic growth overall. The cathodic hydriding was eliminated by a change to Zircaloy specimen holders, but this had no effect on the rate of anodic oxide growth. The latter suggests that the limiting oxide thickness determined by low electronic conductivity of the oxide out-reactor had been relaxed.

These observations allow an understanding of the "Shadow Corrosion" phenomenon in Boiling Water Reactors (BWRs), and suggest that the mechanism of the common nodular corrosion phenomenon in BWRs is a similar process operating on a micro-scale, where the second-phase particles (SPPs) in the zirconium matrix become the "dissimilar metal" in the galvanic couple. This would explain the well known dependence of nodular corrosion on SPP size (i.e. cathode to anode ratio). In Pressurized Water Reactors (PWRs) the galvanic effects appear to be absent because of the high dissolved hydrogen content of the water (all surfaces at the reversible hydrogen potential) and other processes causing degradation of the corrosion resistance of the Zircaloys must be invoked.

Introduction

Ever since zirconium alloys were first developed for use as structural materials in the cores of water cooled nuclear reactors [1] there has been concern that the radiation fields in-reactor would accelerate the corrosion process. Such in-reactor accelerations of corrosion rates have been observed, but there has been little or no agreement on how these accelerations were effected [2], and the number of published papers and reports on the subjects has become legion. A few critical experiments have changed our view of what the important processes are, and may have resulted in a viable hypothesis for these effects.

The corrosion kinetics of zirconium alloys typically exhibit two stages, for alloys such as the Zircaloys and others containing second-phase precipitates (SPPs) of relatively insoluble transition metals such as Fe, Cr, Ni, V etc. The initial stage is a diffusion controlled growth of a thin protective oxide film that follows a kinetic law that is close to cubic, rather than parabolic, at typical water cooled reactor temperatures. Once this oxide exceeds a thickness of about 2 : m this protective film breaks down to give approximately linear kinetics, indicative of a roughly constant thickness residual barrier oxide film. It was expected that reactor irradiation would accelerate both the diffusion controlled growth, and the subsequent breakdown processes [3]. It was therefore something of a surprise when results showed apparently no effect on the pre-transition diffusion controlled processes, and significant accelerations of the post-transition corrosion rates [4,5].

This situation only pertained to behaviour in PWRs (Pressurised Water Reactors), where large concentrations of dissolved hydrogen were present, and the oxide films remained uniform in thickness until oxide spalling ensued at $100 : m. In BWRs (Boiling Water Reactors) where little or no hydrogen was added to the water, and extensive radiolysis of the coolant occurred, the oxide films usually exhibited severely localised nodular corrosion [2]. This behaviour could be controlled by careful attention to the size and distribution of the SPPs [5]. This effect was ascribed to a direct effect of oxidising radicals produced in the water by radiolysis [6]. Although it was evident from early in-reactor loop tests that there was a significant galvanic corrosion component to the formation of nodules, which were observed only under stainless steel grids, and not under Zircaloy grids, on the Zircaloy cladding in a fuel assembly with alternate stainless steel and Zircaloy grids [7]. This aspect of in-reactor corrosion in BWRs was largely ignored until recent severe "shadow corrosion" adjacent to Inconel grids nearly led to fuel failures in the Leibstadt (KKL) BWR [8,9].

Since Zr alloys are usually covered by thick oxide films in-reactor it has always seemed improbable that radiolytically produced oxidising radicals could do anything beyond changing the surface potentials at the oxide film/water surface. Thus, in order to understand this in-reactor behaviour a knowledge of how irradiation affected the transport processes within the zirconia films on the metal surface is needed. Early work [10], recently corroborated [11], showed that the cations in zirconia films were immobile and only the oxygen anions migrated. Charge balance was maintained by electron conduction through what was normally a good electrical insulator [12].

The information needed to formulate a mechanism for the in-reactor corrosion, therefore, comprised a knowledge of which of the transport processes (electronic or oxygen anionic conduction) was rated determining in the absence of irradiation, and the relative effects which in-reactor irradiation had on the two processes. This paper will summarise the evidence obtained on these effects.

Experimental

Measurement of the rate controlling process during oxidation requires a measurement of the potential difference that develops across the oxide film during its growth. The difficulty with such a measurement is the method of applying a contact on the outer surface of the oxide without affecting either of the conduction processes in the oxide [13]. It was decided that this could best be achieved by using an oxygen containing fused salt environment, rather than either an aqueous solution or an outer metallic (or conducting oxide) contact [14]. This allowed measurements to be made at typical reactor temperatures (300-350°C) under conditions where the oxidation rates of zirconium alloys were the same as in high temperature water, but where polarisation of surface reactions in the environment did not affect the results.

Observations of effects of high in-reactor radiation fields on the separate anodic (oxide growth) and cathodic (metal hydriding) processes were made in the ATR at Idaho Falls (USA) during experiments to study the irradiation induced growth of Zircaloys at low temperatures (~ 50°C) in water [15]. Specimens were irradiated initially in aluminum specimen holders, and were later changed to Zircaloy specimen holders. The fast neutron flux (>1 MeV) was $3x10^{14}$ $n.cm^{-2}.s^{-1}$. The oxide film thickness was determined from an interference colour chart after photography through the hot-cell window with a telephoto lens. The specimen was placed on a standard grey background with a colour strip adjacent to it. The colour strip was included in the area photographed and the effect of the lead-glass cell window (yellow) was eliminated by rebalancing the colour of the negative so that the colour strip in the photograph matched the original. Evidence for irradiation damage in the oxide films formed on Zr alloys was obtained by studying the oxides on highly irradiated (10-12 years in-reactor) Zr-2.5%Nb pressure tubes from CANDU reactors in a Philips CM30 transmission electron microscope [16].

Results

The potential across the oxide film formed isothermally on Zircaloy-2 at 300°C always showed the metal to be negative with respect to the oxide/environment surface (Figure 1). The specimen took several minutes to develop a potential of –1.1 V from an initial value close to zero. The origin is not visible in figure 1 because of the logarithmic time scale (but see figure 4, ref.13), as the oxide thickened this potential decreased, but remained negative. These potentials could be materially changed, and even shifted to positive values (Figure 2) by a high temperature (450°C) pre-oxidation, which would have redistributed the iron alloying addition within the oxide formed [17].

In ATR interference-coloured oxides, that increased almost linearly with time, were observed at ~50°C (Figure 3). As the oxide thickened the interference colours changed, but remained relatively uniform over most of the specimen surfaces (Figure 4). Only the oxide on the narrow rim of the specimen that fitted in the slots in the aluminum specimen holders was slightly thinner than on the specimen face. The magnitude of this reduction could not be accurately measured through the hot-cell window because of the small width of this zone and the low magnification.

Subsequent metallographic cross-sections of specimens showed that a rim of hydride had been formed within the region that had been in close proximity to the aluminum specimen holder. This caused a small dimensional change in the specimen that interfered with the accurate measurements of specimen dimensions needed for the irradiation growth determinations (Figure 5). The hydriding of the specimens was eliminated by a change from aluminum to Zircaloy-2 specimen holders for subsequent

irradiation exposures. This did not materially change the rate of growth of the interference-coloured oxide films.

High resolution TEM studies of highly irradiated oxide films have not shown any evidence of irradiation induced point defect clusters or dislocation loops. The oxides appear to have recrystallised in the outer regions (older oxide), but not near the oxide/metal interface. This process must be a solid state process because nanopores are visible (Figure 6), and are thought to be small helium bubbles resulting from the (n,") reaction on ^{16}O [18].

Discussion

The observations of the potentials developed across the oxide during isothermal oxidation experiments show that the electronic conduction through the oxide film is more difficult than the oxygen diffusion that determines the rate of oxide growth. Thus, the negative potential on the metal increases, and accelerates the electron migration (concurrently retarding oxygen ion migration) until the two diffusion processes become equal. A steady potential then persists unless changes in the intrinsic properties of the oxide occur as it thickens. These potentials are determined by the kinetics of the two competing processes, rather than being thermodynamically determined (i.e. they are not the open circuit potential of an electrochemical cell), and can be modified by pre-treatments (such as high temperature pre-oxidation) that alter the balance between the electronic and anionic migration processes.

In the absence of irradiation the electronic resistance is so great that the oxide film is unable to grow thicker than ~2nm without an externally applied anodic potential. The anodic oxide produced grows to a limiting thickness determined by this voltage and the electrolyte in which the anodisation takes place (2.5 – 2.7 nm/V). This is typical of electrolytes in which an impervious barrier film is produced. However, some electrolytes form porous oxide films, which continue to grow in thickness linearly with time [19]. The best known examples of this are oxides grown in nitric acid or nitrate solutions [20]. Under irradiation it appears that the reduced resistivity of the oxide [12] allows the oxide to grow at low temperatures (~50°C) under the potential resulting from the free energy of the oxidation reaction (~2.34V) [13], and that the films that are formed are porous, because the oxide growth continues essentially linearly without saturating. Regrettably, at the time that these specimens were being examined no transmission electron microscopy was carried out because of the very high radiation fields associated with these specimens.

The reduced resistivity of the passive oxides on both zirconium and aluminum also permits the cathodic hydriding of zirconium alloys in contact with aluminum in reactors. This effect has been observed previously in the early severe hydriding of Zircaloy-2 flow tubes in the K-East reactor (KER) at Hanford [21,22]. It was found to be impossible to simulate this galvanic effect in the laboratory in the absence of irradiation. Surprisingly thick interference-coloured oxides were also reported in the KER tubes [23], but the association with the hydriding, and the respective locations of the interference-coloured oxides and the solid hydride were not noted. This work is the first report of the presence of relatively thick oxides and hydride layers at the same location. This indicates that the cathodic hydriding and anodic oxide forming processes operated independently of each other, and with relatively little interaction (as indicated by the slightly thinner oxide on the Zr surfaces in the specimen holder slots). It is well known that zirconia films cannot be reduced electrolytically in neutral aqueous electrolytes, and the magnitude of the oxide thickness reduction in the

slots appears to be compatible with the polarisation curves measured for oxide growth in fused salts [24]. The common facilitating factor for both anodic and cathodic effects is the reduced resistivity of the oxide films in reactor [12].

Application to LWR Conditions

These observations allow both the nodular corrosion and "shadow corrosion" mechanisms in BWRs to be understood. In PWRs the high dissolved hydrogen concentrations in the water eliminate the galvanic potential differences that are necessary in addition to the irradiation enhanced conductivity of the oxide films if enhanced oxide growth is to be observed beyond the interference-coloured oxide region [25] (Figure 7). It appears that, in PWRs, all metals operate at the reversible hydrogen potential [26] so that galvanic potentials between dissimilar metals are absent. In BWRs there is usually insufficient hydrogen added to the water to achieve this situation so that galvanic potential differences remain, and can result in large increases in corrosion rate for Zr alloy components within ~ 5mm. of a dissimilar metal that will anodically polarize them (e.g. stainless steel, nickel alloys). The short range of the effect results from the rather small increase in the water conductivity under irradiation. This, rather than the increased oxide conductivity then becomes the rate limiting step [9]. The "shadow corrosion" phenomena can be readily explained by the above situation. The close similarity of the nodular and shadow corrosion phenomena requires a more micro-mechanistic approach. Although some of the first observations of nodular corrosion showed it to occur only in close proximity to stainless steel grids, with material that was very susceptible to nodular corrosion [27] the nodules were often fairly uniformly distributed over the Zircaloy-2 surfaces between the grids. The sensitivity to nodular corrosion was heavily dependent on the precise fabrication route that had been followed for the batch of cladding [28]. This sensitivity to nodular corrosion could be correlated with the second phase particle (SPP) size in the alloy. The number of nodules, however, was always far fewer than the number of SPPs per unit area of surface. Thus, some other selection rule (in addition to just the particle size) was needed to specify the locations at which a nodule would nucleate. Many suggestions have been made for what this selection rule might be [2], but the frequency of clusters of closely spaced SPPs seems to be a preferred one [29].

The close similarity between the galvanic factors in nodular and shadow corrosion suggests that nodular corrosion is a micro-version of shadow corrosion. In the initiation of a nodule then; the area of the " - Zr matrix around a large SPP or cluster of SPPs would be the anode and the SPPs would be the cathode. For a given SPP composition then the galvanic potential difference with the matrix would be set and the magnitude of the anodic current would be determined by the cathode area (i.e. the SPP size, or cluster size). Changes in fabrication route, which changed the SPP composition, could change the galvanic potential available, and (for otherwise similar SPP size and distribution) hence change the susceptibility to nodular corrosion. At present, there is insufficient data on SPP/matrix potential differences to allow this hypothesis to be thoroughly tested. It does, however, provide a rationalisation for many of the observations. The observation that hydrogen uptake by batches of cladding showing severe nodular corrosion was not significantly different from that of well behaved batches, is matched by the absence of enhanced hydrogen uptake in the area of severe shadow corrosion in KKL. In both instances the cathodic hydrogen evolution process was occurring at the cathodes and hydrogen was not entering the Zr. Other observations that is compatible with this hypothesis include:-

1. Absence of nodular corrosion, but enhanced uniform corrosion, for material with very small SPPs [28]. These SPPs dissolve rapidly by Fe recoil from fast neutron collisions [30] and result in enhanced uniform corrosion in post-irradiation laboratory tests, and are probably one cause of the accelerated corrosion in PWRs when oxide thicknesses exceed ~ 10 : m.

2. Zr-Nb alloys (both 1%Nb and 2.5%Nb) that do not contain SPPs of the type present in Zircaloys do not suffer from nodular corrosion unless the Fe impurity level is very high.

3. The absence of visible radiation damage in oxide films on zirconium alloys implies no direst acceleration of in-reactor corrosion due to enhanced diffusion in the oxide. Thus, reduced in-reactor corrosion rates become possible if the in-reactor annealing of the metal structure results in improved corrosion resistance [31].

Conclusions

In-reactor observations of enhanced oxide growth rates and simoultaneous severe hydriding of Zircaloy specimens shows that the anodic and cathodic processes follow independent mechanistic rules. The key to understanding these phenomena is the enhanced electrical conductivity of the oxide films under irradiation, and the persistence of galvanic potentials between dissimilar metals if the reactor water contains insufficient dissolved hydrogen. No evidence has been found for irradiation damage in zirconia films resulting from fast neutron collisions. Only nanometric helium bubbles resulting from the transmutation of ^{16}O by the (n,") reaction are visible. These factors permit the prevalent observation of "shadow corrosion" in BWR water chemistries. Severe examples of this are fortunately infrequent. Since SPPs are galvanically dissimilar to the zirconium matrix it is concluded that nodular corrosion is merely a microscopic variant of shadow corrosion. In the absence of Fe containing SPPs, or after the irradiation induced dissolution of very small SPPs, nodular corrosion should be absent. However, irradiation enhanced dissolution of SPPs should lead to enhanced uniform corrosion in BWRs and PWRs where this phenomenon will degrade the corrosion resistance of the alloy.

References

1. H.G. Rickover, L.D. Geiger and B. Lustman, "History of the development of zirconium alloys for use in nuclear reactors", U.S. Report, Division of Naval Reactors, Washington, DC, TID-26740, March 1975.
2. "Waterside corrosion of zirconium alloys in nuclear power plants", International Atomic Energy Agency, Vienna, Austria, TECDOC-996 (1998).
3. B. Cox, J. Nuclear Mater., 28 (1968) 1-47.
4. E. Hillner, "Long-term in-reactor corrosion and hydriding of Zircaloy-2 tubing", Proc. 5th Int. Conf. on Zr in the Nuclear Ind., Boston, U.S., ASTM-STP-754, (1982) 450-478.

5. F. Garzarolli, T. Broy and R.A. Busch, "Comparison of the long-term behavior of certain zirconium alloys in PWR, BRW and laboratory tests", Proc. 11th Int. Symp. on Zr in the Nuclear Ind., Garmisch-Partenkirchen, Ger., ASTM-STP-1295 (1996) 850-864.
6. W.G. Burns and P.B. Moore, "A survey of in-reactor zirconium alloy corrosion", Proc. BNES Conf. on Water Chemistry of Nuclear Reactor Systems, Bournemouth, UK., 1977, pp 281-289.
7. R. Sumerling, A. Garlick, A. Stuttard, J.M. Hartog, F.W. Trowse and P. Sims, "Further evidence of Zircaloy corrosion in fuel elements irradiated in a steam generating heavy water nuclear reactor", Proc. 4th Int. Conf. on Zr in the Nuclear Ind., Stratford-upon-Avon, U.K., ASTM-STP-681 (1979) 107-121.
8. H-U. Zwicky, H. Loner, B. Andersson, C-G. Wiktor and J. Harbottle, "Enhanced spacer shadow corrosion on SVEA fuel assemblies in the Liebstadt nuclear power plant", Proc. ANS Int. Topical Meeting on LWR Fuel Performance, Park City, UT, (2000), Vol.1, 459-469.
9. A. Chatelain, B. Andersson, R-G. Ballinger and G. Wikmark, "Enhanced corrosion of zirconium-based alloys in proximity to other metals", ibid., 485-498.
10. J.L. Whitton, J. Electrochem. Soc., 115 (1968) 58-60.
11. U. Brossmann, R. Whrscheim, U. S`dervall and H.E. Schafer, J. Appl. Phys., 85 (1999) 7646-7654.
12. D.W. Shannon, "Electrical properties of ZrO_2 corrosion films", Proc. USAEC Symp. on Zirconium Alloy Development, Castlewood, CA, G.E. Report GEAP-4089, Vol.II, Paper 18 (1962).
13. D.H. Bradhurst, J.E. Draley and C.J. van Drunen, J. Electrochem. Soc., 112 (1965) 1171-1177.
14. B. Cox, J. Nuclear Mater., 31 (1969) 48-66.
15. B. Cox and V. Fidleris, "Enhanced low-temperature oxidation of zirconium alloys under irradiation", Proc. 8th Int. Symp. on Zr in the Nuclear Ind., San Diego, CA, ASTM-STP-1023, (1989) 245-265.
16. O.T. Woo, Y-P. Lin and D. Khatamian, "Oxide microstructure and deuterium ingress in Zr-2.5%Nb CANDU Pressure Tubes", Proc. 5th Int. Conf. on Microscopy in Oxidation, Limerick, Eire, Aug. 2002, to be published.
17. B. Cox and H.I. Sheikh, J. Nuclear Mater., 249 (1997) 17-32.
18. I. Muir, W.H Hocking, D. Khatamian and V.F. Urbanic, "Elucidating oxidation mechanisms of irradiated zirconium alloys using surface analytical methods", Proc. 10th Int. Conf. on Environmental Degradation of Materials in Nuclear Power Systems – Water Reactors, Lake Tahoe, (2001) C.D.
19. R.D. Misch, "Electrode reactions of zirconium metal", Chapter 11-V, Metallurgy of Zirconium, Eds. B. Lustman and F. Kerze Jr., McGraw-Hill, NY, (1955) 663-677.
20. B. Cox, J. Electrochem Soc., 117 (1970) 654-664.
21. W.K. Alexander, "Hydriding of Hanford production reactor process tubes", paper presented at ANS Conf. on Reactor Operating Experience, Atlantic City, NJ, (1967) and Report DUN-SA-34 (1967).
22. W.K. Winegardner and B. Griags, "Zirconium hydride formation in Hanford production reactor process tubes", U.S. Report BNWL-588, Battelle North-West Laboratory, Richland, WA, 1967.

23. A.B. Johnson, Jr., "Zirconium alloy oxidation and hydriding under irradiation: Review of Pacific Northwest Laboratories' test program results", U.S. Report, EPRI-NP-5132, Electric Power Research Inst., Palo Alto, CA, 1987.
24. W. Hhbner and B. Cox, "Electrochemical properties and oxidation of some zirconium alloys in molten salt at 300-500°C", Canadian Report, AECL-4431, Chalk River, ON, (1973).
25. R.C. Asher and B. Cox, "The effects of irradiation on the oxidation of zirconium alloys", Proc. IAEA Conf. on Corrosion of Reactor Materials, Salzburg, AU, 1962, STI Pub.59, Vol.2, 209-221.
26. B. Rossberg and A. Molander, "In-plant corrosion potential monitoring", Proc. IAEA Tech. Comm. Meeting, Ìeñ, Czech Rep., 1993, IAEA-TECDOC-927, pp.331-339.
27. Papers from Session on Nodular Corrosion, Proc. 7th Int. Symp. on Zr in the Nuclear Industry, Strasbourg, FR., ASTM-STP-939 (1987).
28. F. Garzarolli, R. Schumann and E. Steinberg, "Corrosion optimised in Boiling Water Reactor fuel elements", Proc. 10th Int. Symp. on Zr in the Nuclear Industry, Baltimore, MD, ASTM-STP-1245 (1994) 709-723.
29. P. Rudling and B. Lehtinen, "Mechanistic understanding of nodular corrosion", Electric Power Research Inst., Palo Alto, CA, Report EPRI-TR-103396 (1993).
30. X. Iltis, F. Lefebvre and C. Lemaignan, "Microstructure evolution and iron redistribution in Zircaloy oxide layers : Comparative effects of neutron irradiation flux and irradiation damages", Proc. 11th Int. Symp. on Zr in the Nuclear Industry, Garmisch-Partenkirchen, GER, ASTM-STP-1295 (1996) 242-264.
31. O.T. Woo, G.M. McDougall, R.M. Hutcheon, V.F. Urbanic, M. Griffiths and C.E. Coleman, "Corrosion of Electron-Irradiated Zr-2.5Nb and Zircaloy-2", Proc. 12th Int. Symp. on Zr in the Nuclear Industry, Toronto, ON, ASTM-STP-1354 (2000) 709-734.

Figure Captions

1. Potential/time curves for Zircaloy-2 in fused salt at 275-445°C.
2. Effect of pre-oxidation at 445°C on potential/time curves at 275°C.
3. Plot of oxide thickness vs fast neutron dose in ATR.
4. Visual appearance of "anodic" oxide formed at 50°C in ATR.
5. Hydride layers formed in ATR during exposure in Al specimen holders
   a. Typical hydride layer, b. Thickest hydride observed.
6. Crystallite boundary cracks and nanopores observed in oxide films on Zr-2.5%Nb pressure tube B1W19.
7. Oxidation of Zircaloy-2 in irradiated steam at 350°C.

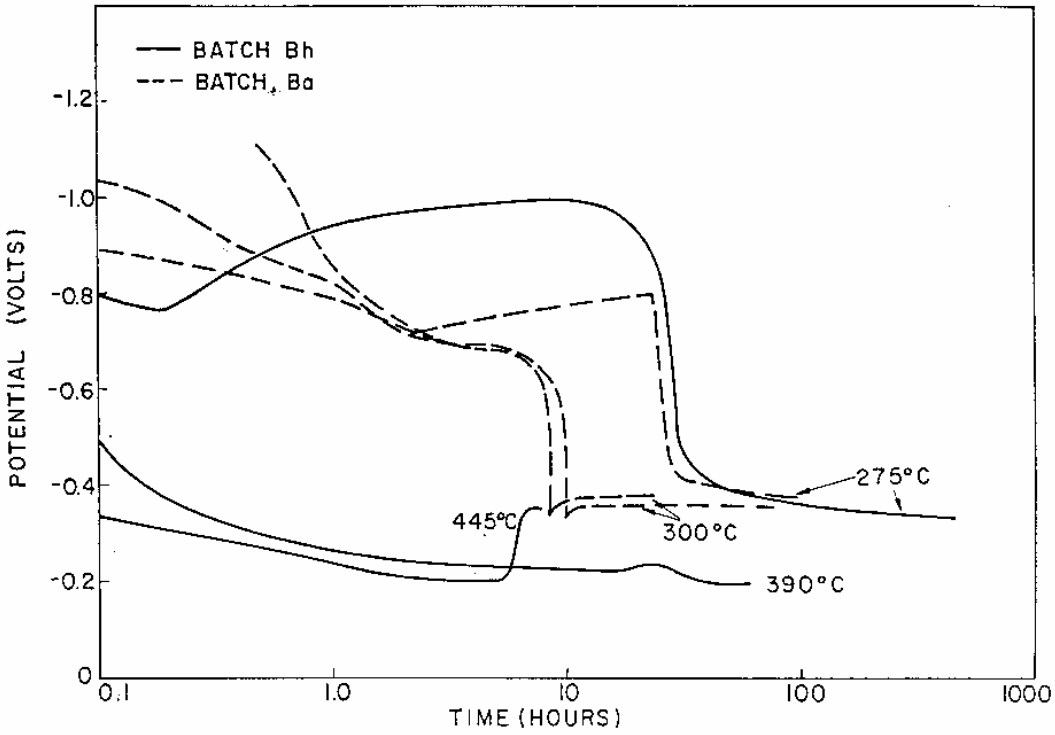

Fig. 1. Potential versus time curves for Zircaloy-2 in fused salt.

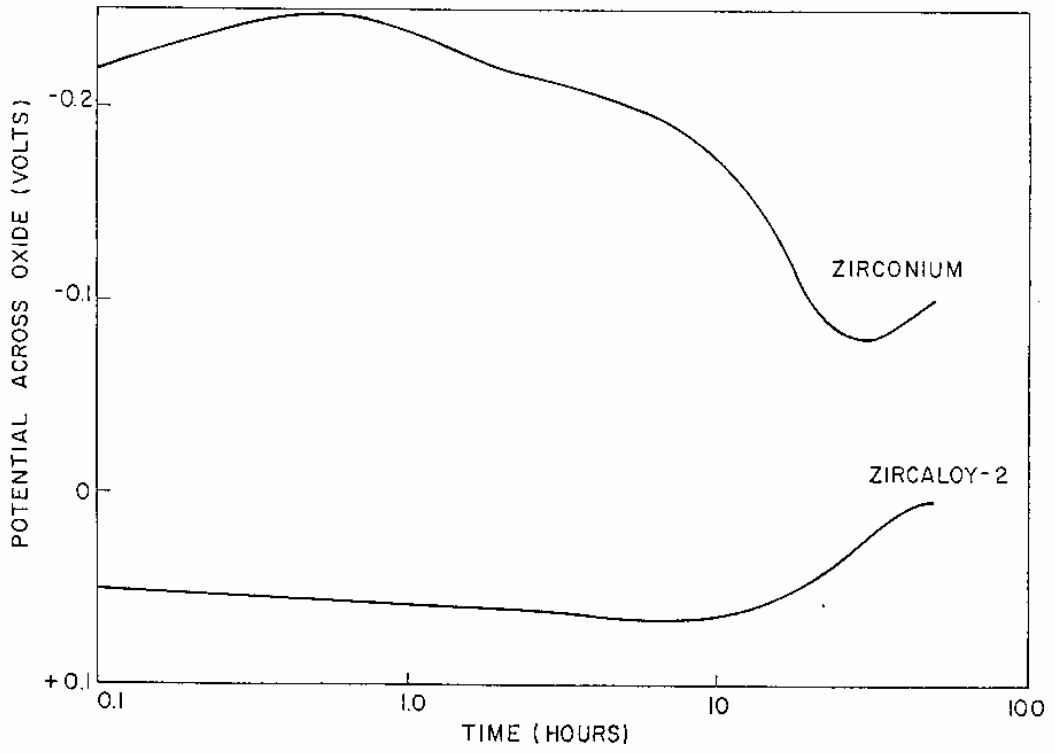

Fig. 2 Potential versus time curves at 275 °C for specimens preoxidised at 445 °C.

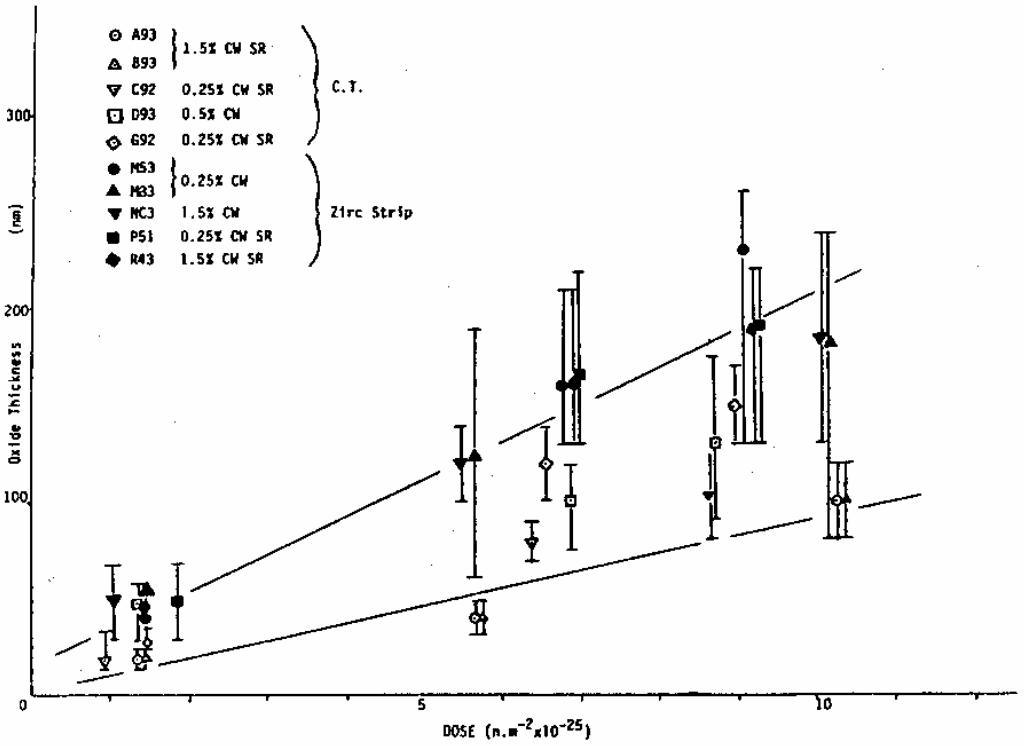
A93
B93
1.5% CW SR
C92 0.25% CW SR
D93 0.5% CW
G92 0.25% CW SR
C.T.
MS3
M33
0.25% CW
MC3 1.5% CW
P51 0.25% CW SR
R43 1.5% CW SR
Zirc Strip
Oxide Thickness (nm)
300
200
100
0
5
10
DOSE (n.m^{-2}x10^{-25})

Fig. 3.

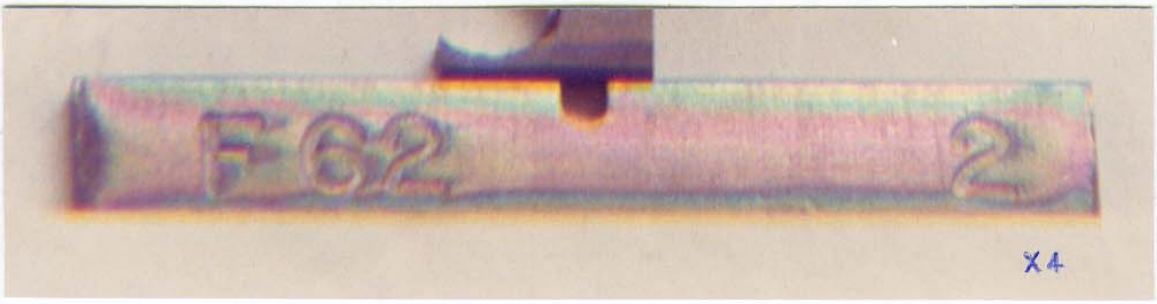

Fig.4.

a.

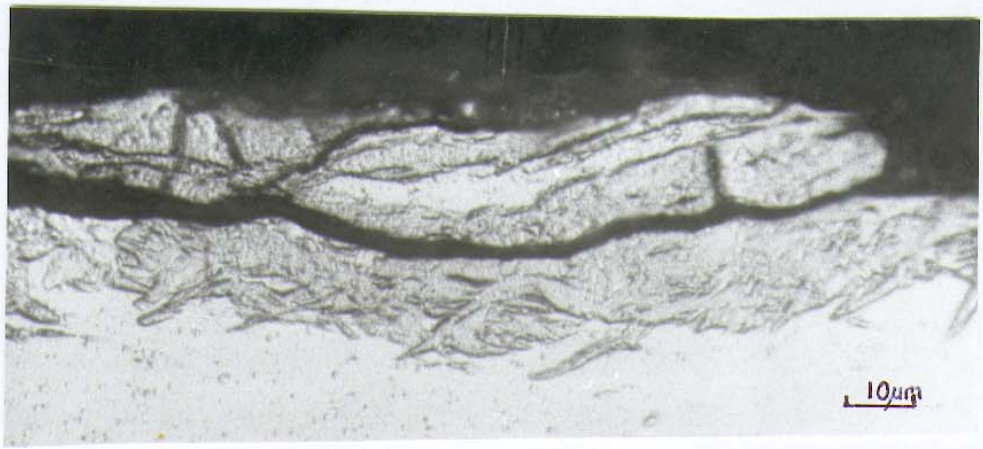

b.

Fig.5.

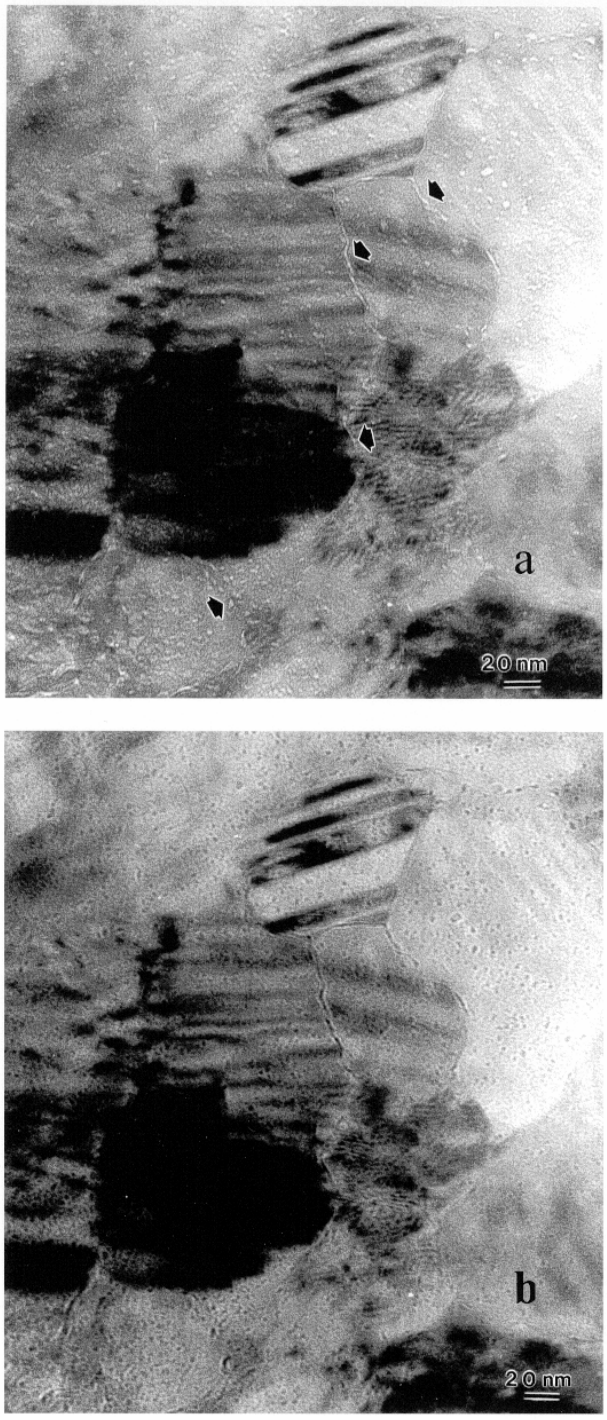

Figure 6(a) and (b). Under- and over-focussed images of equiaxed grains near the surface region of an oxide made from B1W19 at the 5 m location, showing nanopores and cracks (arrowed) at grain boundaries.

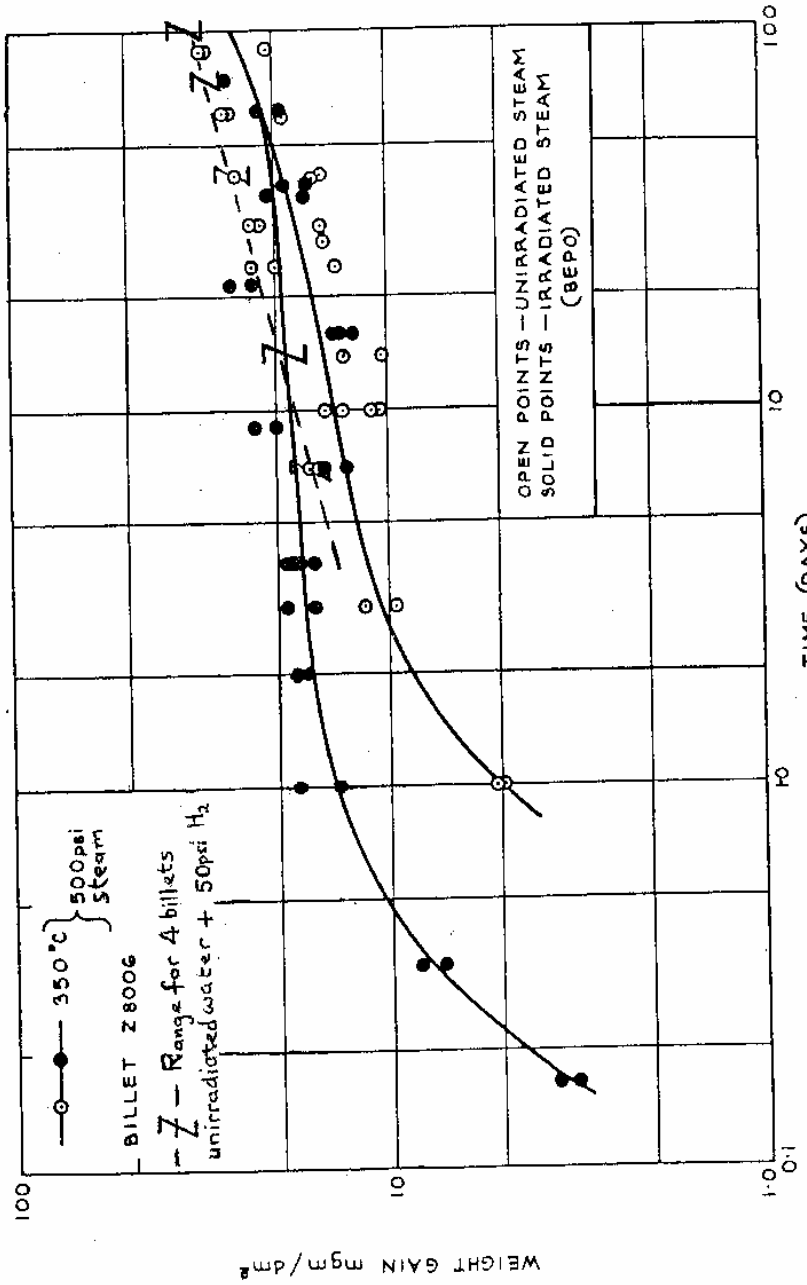

Fig 7. OXIDATION OF ZIRCALOY-2 IN IRRADIATED STEAM AT 350°C.